CDS 232
Final Project

Noel Csomay-Shanklin

03/20/2020

1 Introduction

Throughout this report, we will be investigating the nonlinear dynamic system that is the n-pendulum – a depiction of this system can be found in Figure 1. Seeing as though the pendulum is the canonical nonlinear system, and the double pendulum is a classic example of chaos theory, the natural extension is to propagate the system into n-dimensions. Specifically, it will be interesting the investigate "how nonlinear" the systems are with respect to the parameter n. For example, an investigation of the Lipschitz constant will reveal the the double pendulum is much more sensitive to initial conditions and parameters than the single pendulum. In the proposed framework, this easily can be investigated into as many dimensions is desired. This system is also personally interesting because it is loosely related to the research of walking robots; legged locomoters are simply series pendula.

The equations of motion for the n-pendulum are derived in the appendix, and are given by (1). This system is stable about the $\mathbf{0}$ fixed point and therefore requires no controller to render stability. In fact, with nonzero b_i terms, it is asymptotically stable about the origin. This system also sets itself up well for the controls project of the next quarter, with the ability to investigate how control inputs on various links (fully and under actuated cases) effect the behavior of the overall system. The code to perform this derivation has already been developed, with the time to derive the equations of motion and simulate a set of initial conditions for a small time interval given in Table 1.

Table 1: Time taken to derive equations of motion for various n-pendula and simulate a given trajectory.

n	Time (s)
1	0.5
2	1
3	1.5
40	2.2
5	3.1
10	13.5
15	35.3
20	77
30	256

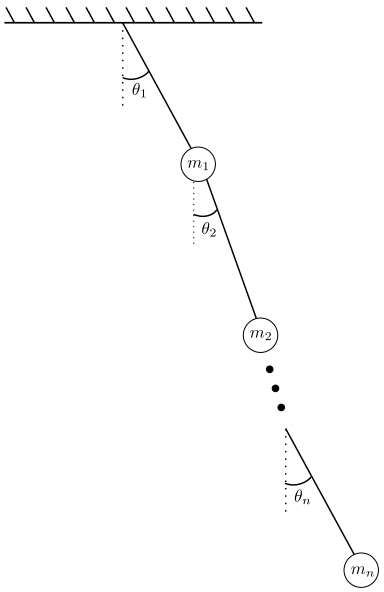

Figure 1: The n-Pendulum. The i^{th} link has mass m_i, length l_i, angle off of global vertical θ_i, and damping coefficient b_i.

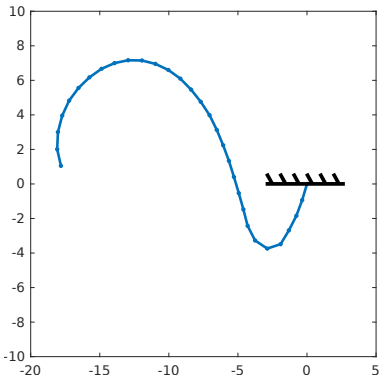

Figure 2: Simulation of the 30-Pendulum from a random initial condition.

$$l_i^2\ddot{\theta}_i\sum_{j=1}^{n}m_j+l_i\sum_{j=1}^{n}\sum_{k=\max\{i,j\}}^{n}l_jm_k(\ddot{\theta}_j\cos(\theta_i-\theta_j)-\dot{\theta}_j(\dot{\theta}_i-\dot{\theta}_j)\sin(\theta_i-\theta_j))(1-\delta_{ij})$$
$$-gm_i\sum_{j=1}^{i}l_j\sin\theta_i+l_i\dot{\theta}_i\sum_{j=1}^{n}\sum_{k=\max\{i,j\}}^{n}l_j\dot{\theta}_jm_k\sin(\theta_j-\theta_i)(1-\delta_{ij})=b\dot{\theta}_i \tag{1}$$

2 Setup

Let $\theta \in \mathcal{Q} = \mathbb{S}^n$ represent coordinates in the configuration space of the system and $x = [\theta\ \dot{\theta}] \in T\mathcal{Q} \simeq \mathbb{S}^n \times \mathbb{R}^n$ represent the full state of the system. Now consider the equations of motion of the $n-pendulum$ as

$$\dot{x} = f^n(x),$$

where $f^n : T\mathcal{Q} \to \mathbb{R}^n$. For the sake of simplicity, we will let $g = 9.81$, $m = 1$, $l = 1$, and $b = -0.1$ for all future discussions, unless otherwise stated.

3 Lipschitz Constant

Because f^n is continuously differentiable, we can employ Theorem 2.2 to conclude that our system is Locally lipschitz continuous for all values of n. In the case where $n = 1$, we can perform a calculation of the Lipschitz constant by hand. Consider f^1 as

$$\dot{x} = f^1(x) = \begin{bmatrix} x_2 \\ -g\sin(x_1) - \frac{x_2}{10} \end{bmatrix}$$

in the following progression

$$\begin{aligned} &\|f^1(x) - f^1(\tilde{x})\| \\ &\quad = \left\| \begin{bmatrix} x_2 - \tilde{x_2} \\ -g(\sin(x_1) - \sin(\tilde{x_1})) - \frac{1}{10}(x_2 - \tilde{x_2}) \end{bmatrix} \right\|. \end{aligned}$$

We now employ the following theorem without proof.

Theorem 3.1. *A function $f : \mathbb{R}^n \to \mathbb{R}^n$ is locally (globally) Lipschitz iff each $f_i : \mathbb{R}^n \to \mathbb{R}$ is locally (globally) Lipschitz.*

With this, consider f_1^1 as

$$\begin{aligned} \|f_1^1(x) - f_1^1(\tilde{x})\| &= \|x_2 - \tilde{x_2}\| \\ &= \| \begin{bmatrix} 0 & 1 \end{bmatrix} (x - \tilde{x})\| \\ &= \underbrace{1}_{L} \|x - \tilde{x}\|. \end{aligned}$$

In addition, we have

$$\begin{aligned} &\|f_2^1(x) - f_2^1(\tilde{x})\| \\ &\quad = \| - g(\sin(x_1) - \sin(\tilde{x_1})) - \frac{1}{10}(x_2 - \tilde{x_2})\| \\ &\quad \leq \| - g(x_1 - \tilde{x_1}) - \frac{1}{10}(x_2 - \tilde{x_2})\| \\ &\quad \leq \underbrace{g}_{L} \|x - \tilde{x}\|. \end{aligned}$$

Therefore, with $L = \max\{1, g\}$, we have that our system is globally Lipschitz.

As a precursor to higher dimensional cases, we can set up the problem of finding the Lipschitz constant as a maximization problem, and compute the answer numerically via the following program

$$L_0^n = \max_{x \in B_\epsilon(x_0)} \|Df^n(x)\|,$$

where $\|\cdot\|$ is selected to be the 2-norm. This can be run with lower and upper bounds imposed on the `fmincon` function in Matlab in order to restrict the domain to B_ϵ. When run in the $n = 1$ case, we return 9.81, as expected. Additionally, this bound is found even when $\epsilon \to \infty$, leading us to believe that this bound is really a global Lipschitz constant rather than a local one, as was previously proven. In the case when $n = 2$, this evaluation becomes unbounded; therefore, we can reasonable conclude that for $n > 1$, only local Lipschitz continuity holds. This matches intuition, because in higher dimensional cases, coupling between links leads to $\dot{\theta}^2$ terms, which are not globally Lipschitz functions. The Lipschitz constants of various n-pendula when $\epsilon = 1$ are summarized in Table 2. The trend of higher n causing higher L_0 is expected; as n increases, the chaos and "speed" of the system also increases, meaning that the states are more likely to change rapidly.

Table 2: Local Lipschitz constants for various n values

n	L_0
2	40.0
3	76.8
4	119.8

4 Picard Iteration

A numerical instantiation of the Picard integral was implemented in Matlab and is used to solve the solutions of various n cases with the initial condition $\theta_i = 2$, $\dot{\theta}_i = 0$. The Picard integral was left to iterate until subsequent z values were within 0.001 of each other, i.e. the algorithm converged.

As can be seen in Figure 3, for the $n = 1$ case, the discrete dynamics system as described by the Picard operator converge to a solution that matched ODE45 within discernable error. The iterations of the algorithm can be seen in Figure 3a where lines that are more red correspond to earlier fits (of lower polynomial order) and lines that are more green correspond to later fits. In fact, T could be extended arbitrarily far and the solution would match ODE45 exactly if the algorithm were left to converge.

This was not the case for higher values of n, as seen in Figure 4 when $n = 2$. Even though the algorithm converges, the solution diverges from ODE45 over time. The explanation for this is from the chaotic nature of the system. Any numerical difference that develops over time will be compounded buy the chaotic nature of the double pendulum and will lead to divergent solutions. We can also look at Figure 4a to see that although the algorithm converges, its intermediate states oscillated wildly at the end point. In fact, if we extended the time interval further, the algorithm would diverge and no solution could be found. To ameliorate this, we implemented an iterative Picard method that would only solve the system for 0.1 seconds and would then pass that final condition to be the initial condition of the next iteration. This allowed for great computational speedup, and reasonable solutions could be found (over small time intervals) in the case where $n = 2$. In fact, this method allowed for solutions to be found in the $n = 4$ case, as seen in Figure 5, which would otherwise have been intractable to compute in a reasonable amount of time with the base Picard Iteration method. As can be seen in Figure 5b though, this method is still not rigorous to increased time intervals. If this method were used moving forward, smaller time intervals or adaptive time intervals could have been used to acheive more accurate results.

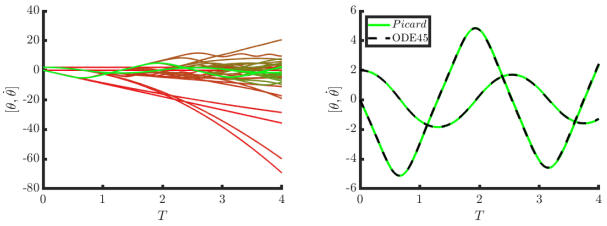

(a) Iterations of Picard (b) ODE45 vs Picard

Figure 3: Picard Integral for $n = 1$, $T = 4$.

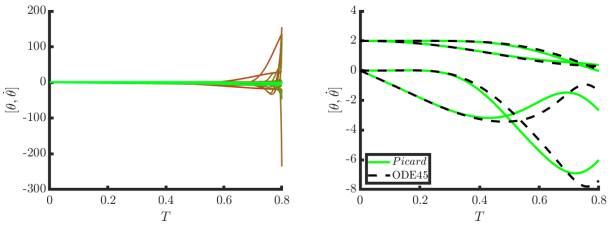

(a) Iterations of Picard (b) ODE45 vs Picard

Figure 4: Picard Integral for $n = 2$, $T = 0.8$.

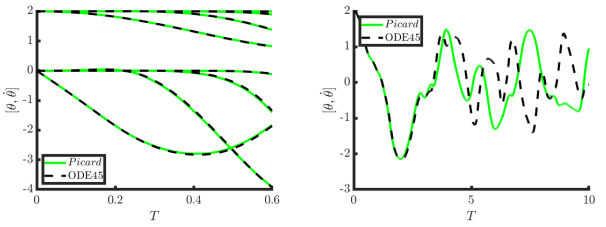

(a) ODE45 vs Picard, T=0.6 (b) ODE45 vs Picard, T=10

Figure 5: Picard Integral for $n = 4$, varying time scales.

5 Perturbation

5.1 Initial Condition

In order to gain an intuition of the dynamics, we will start with the $n = 1$ case. We assume $q(t_0) = [2\ 0]^\top$ for the nominal system, and $\tilde{q}(t_0) = [4\ 0]^\top$ for the perturbed system. As can be seen in 6, even with a large

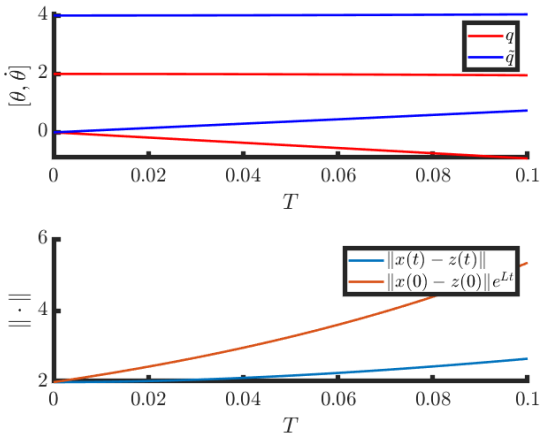

Figure 6: Sensitivity to Initial Conditions for $n = 1$. q is the nominal system and $\tilde{q}$ is the perturbed system.

perturbation in the initial condition, the norm of the error is bounded by $\|x(0) - z(0)\|e^{Lt}$, as is predicted by the theory. Because the Lipschitz constant is so large even for this simple system, the dynamics were only simulated over a small time interval. Moving onto the triple pendulum with the same perturbation in initial condition, we get similar behavior, as seen in Figure 7. This plot is perhaps less interesting because the Lipschitz constant is so massive that it creates an insurmountable bound. Because we are discussing sensitivity to initial conditions, we will take a slight excursion into chaos theory just for fun. We simulate 120 triple pendula for 5 seconds with initial conditions within some $\epsilon = 0.01rad$ ball, and plot the con-

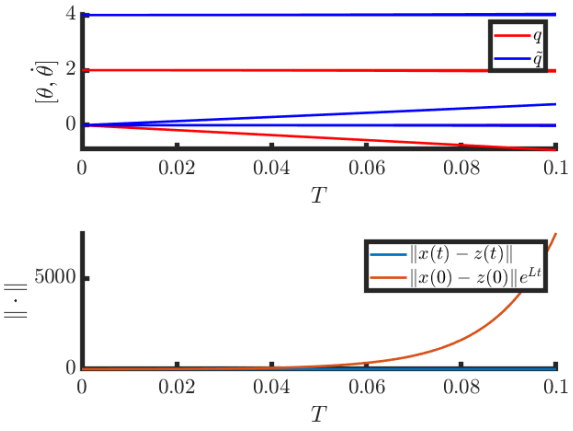

Figure 7: Sensitivity to Initial Conditions for $n = 3$. q is the nominal system and $\tilde{q}$ is the perturbed system.

figuration space of the resulting dynamics, as seen in Figure 8. It is color coded based on time; more blue means t is closer to 0, and more red means t is closer to 5. Each blue point at the head of the line represents a different initial condition. It is interesting to watch this plot evolve over time, which can be found here. The time evolution of two instances of the physical system can be found here. Figure 8 reveals two

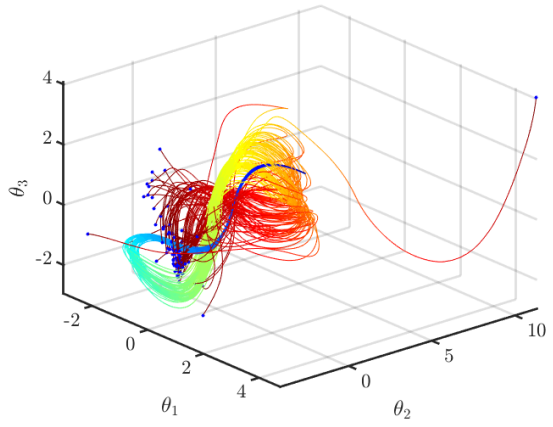

Figure 8: Flow of the system in configuration space depicting sensitivity to initial conditions.

things. First, the system is highly chaotic, because even after just 5 seconds the various pendula have wildly diverged. Second, the Lipschitz constant is a rediculously conservative bound on the error. Even though the system is chaotic, for the first few seconds the dynamics are closely related, a fact which is not at all captured by the bound.

5.2 System Parameters

Again, we will start by considering the single pendulum, as shown in Figure 9. In the following discussion, $\tilde{q}$ will be the solution of the system with perturbed parameters. Our initial system has the same parameters as were described in Section 2, and the perturbed system has the following parameters: g = 19.81 m/s, m = .1, b = 0, l = 0.1 (over 100% different). Similar to before, in the $n = 3$ case not

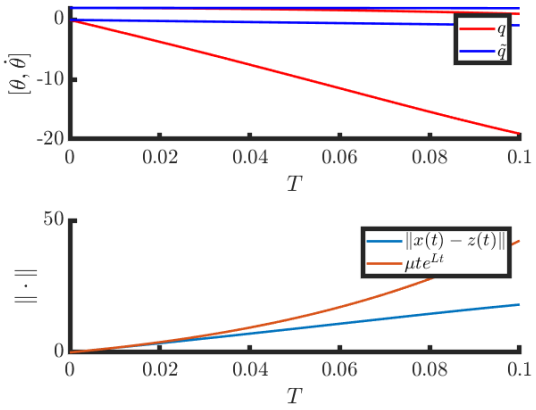

Figure 9: Sensitivity to Parameters for $n = 1$. q is the nominal system and $\tilde{q}$ is the perturbed system.

much useful is gained from the Lipschitz constant, as is seen in Figure 10. In order to derive the constant μ such that the norm of the perturbation dynamics satisfies the bound $\|g(z)\| \leq \mu$ for all $z \in E$, the same strategy is used as with calculating the Lipschitz constant. Dynamics for g are generated by subtracting the nominal dynamics from the perturbed dynamics, and `fmincon` is used to find the maximum norm of g in the domain. A table showing the values of μ is summarized below, where similar to L_0, the trend is linear with respect to n.

Table 3: Local Lipschitz constants for various n values

n	μ
1	158.5
2	231.6
3	286.7
4	338.3

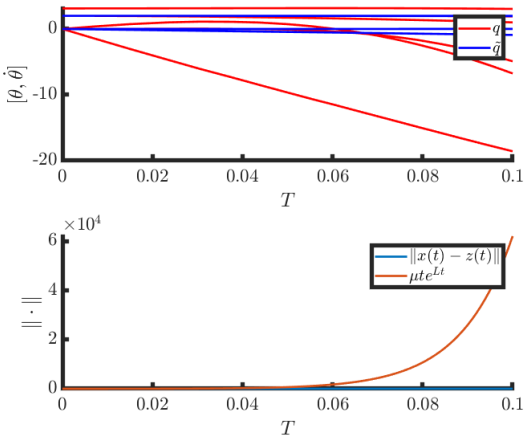

Figure 10: Sensitivity to Parameters for $n = 3$. q is the nominal system and $\tilde{q}$ is the perturbed system.

6 Equilibrium Points

We propose the family of points $x = [n\pi, 0] \in \mathbb{R}^{2n}$, $n \in \mathbb{Z}^n$ as equilibrium point candidates for the n-pendulum. Plugging this into 1 results in the following equation

$$l_i^2 \ddot{\theta}_i \sum_{j=1}^{n} m_j \pm l_i \sum_{j=1}^{n} \sum_{k=\max\{i,j\}}^{n} l_j m_k \ddot{\theta}_j (1 - \delta_{ij}) = 0$$

where the sign of the second term is dependent on the inputs. It is easy to see this can only be true for every $i \in [1, .., n]$ if $\ddot{\theta}_i \equiv 0$. Therefore, we have that $\dot{x} = f(x) = 0$, implying that $x = [n\pi, 0] \in \mathbb{R}^{2n}$, $n \in \mathbb{Z}^n$ are equilibrium points of the n-pendulum for all n, of which intuition tells us only $0 \in \mathbb{R}^{2n}$ is stable.

7 Lyapunov

For the following analysis, we will restrict ourselves to the point $0 \in \mathbb{R}^{2n}$. We propose the total relative energy of our system as a Lyapunov function candidate for the point $0 \in \mathbb{R}^{2n}$, i.e.

$$V(x) = E(x) - E(0) = T(x) + V(x) - V(0).$$

This choice of Lyapunov function is obviously locally positive definite by noting that T contains a quadratic term in $\dot{\theta}$ and the first order Taylor approximation of $\cos(\theta)$ is on the order of $-\theta^2$, whereby $-V(x)$ is positive definite. Due to the complexity of solving the $\dot{V}$, a symbolic approach was taken in MATLAB, i.e. V was constructed along with the equations of motion and $\dot{V} = \frac{\partial V}{\partial x} f(x)$ was calculated. The results are summarized in Table 4. More values were not calculated because of the computational complexity

Table 4: $\dot{V}$ for various n values

n	$\dot{V}(x)$
1	$b_1\dot{\theta}_1^2$
2	$b_1\dot{\theta}_1^2 + b_2\dot{\theta}_2^2$
3	$b_1\dot{\theta}_1^2 + b_2\dot{\theta}_2^2 + b_3\dot{\theta}_3$
4	$b_1\dot{\theta}_1^2 + b_2\dot{\theta}_2^2 + b_3\dot{\theta}_3^2 + b_4\dot{\theta}_4^2$

of solving the equations of motion in explicit form, but the trend is clear. We can make the following conjecture

$$\dot{V}_n = \sum_{i=1}^{n} b_i \dot{\theta}_i^2,$$

which the numeral results allude to the validity of. This conclusion is corroborated by the development in class, where the above form was shown the be valid for mechanical systems. Therefore, because $\dot{V}$ is negative definite for any negative choice of b_i, we can conclude that the origin is stable. We now employ La Salle's invariance principle to show that the origin is in fact asymptotically stable. Fix any n, and assume $\dot{V}_n = \sum_{i=1}^{n} b_i \dot{\theta}_i^2$. If $\dot{V}_n = 0$, it must be true that $\dot{\theta}_i \equiv 0$. This implies from our dynamics that

$$-gm_i \sum_{j=1}^{i} l_j \sin\theta_i$$

must be zero, which is only true for all i if each θ_i is some multiple of π. From the locality of our Lyapunov function, we can restrict this to requiring θ_i to be zero, i.e. $x = 0$. Thus, from La Salle's invariance principle, we have the the origin is asymptotically stable. Visualizations of the flows along Lyapunov surfaces for the 1, 2, and 3 dimensional cases can be found here, here, and here, respectively.

8 Region of Attraction

In order to estimate the region of attraction, the linearization method described in chapter 8 is employed. This is done numerically as to allow for scaling up in dimensionality. After the linearization of the system $Df(x)$ is constructed, $G(x) = \int_0^1 Df(\tau x)d\tau - Df(0)$ can easily be calculated. Additionally, using the `lyap` function in Matlab, the continuous time Lyapunov equation can be used to solve for the P corresponding to $Q = I$, resulting in an upper bound for N, i.e.

$$N_{max} = \frac{1}{2\lambda_{max}(P)}.$$

Then, `fmincon` is used to solve the following optimization problem

$$\begin{aligned} \max_{x \in TQ} \quad & \|G(x)\|_2 \\ \text{s.t.} \quad & \|G(x)\|_2 < N_{max}. \end{aligned}$$

We can use $r = \|x^*\|_2$ where x^* is the argmax of the above optimization problem to construct a ball around the origin $B_r(0)$ to estimate our region of attraction. As a sanity check, for the $n = 1$ case with $g = l = b = 1$, the value $r = 1.35$ was found, which matches very closely to what was given in the book. Using our normal paraemeters as described in Section 2, the following table summarizes our region of attraction for various n values.

Table 5: Domain of attraction for various n values

n	r
1	0.0752
2	0.0115
3	0.0057

These results are, however, quite dissatisfying. Turning to the literature to investigate other ways to estimate domains of attraction reveals that we can use the method of reverse integration of our solutions to expand an opproximation of our domains of attraction. We start by constructing a level set of our Lypapunov function

$$\Omega_\epsilon = \{x : V(x) \leq \epsilon\}.$$

Because of the asymptotic stability of the origin, we know that this set will be forward invariant, and that the ω-limit set is the origin. This implies that in reverse time, this set is backwards invariant. Therefore, in order to expand this set, we sample points along it's boundary and integrate in reverse time. We need not select points in the interior, because the interior points must necessarily cross the boundary first in reverse time. For the $n = 1$ case, choosing $\epsilon = 0.0752$, our previous estimate of the domain of attraction, we have the image seen in 11 where each colored line represents the "reverse" flow of a different initial condition. Although this is not a valid proof of a larger domain of attraction, it seems as though we are sweeping out a new, larger area, namely that $\Omega_{0.2}$ could serve as a domain of attraction. If we now take points at the maximal radius, $\Omega_{0.2}$, and repeat the process iteratively, we get something more interesting, as seen in Figure 12. This image is a bit misleading, however. Here, one would assume that once past a certain radius, only a small subset of points converge to the origin. This is simply due to the

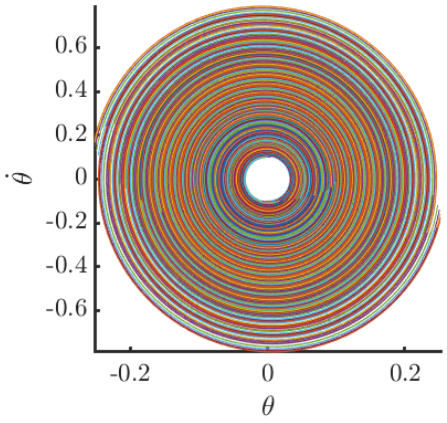

Figure 11: $\Omega_{0.1}$

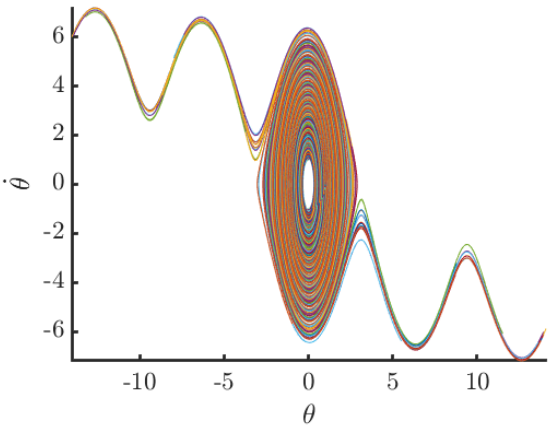

Figure 12: Ω_1

fact that we are representing the phase space in the wrong geometry. Specifically, we are attempting to map $\mathbb{S} \times \mathbb{R}$ to $\mathbb{R}^2$, which are most certainly not homeomorphic. In order to better understand our set, we therefore use the mod function to map all points to the interval $[0, 2\pi)$. This results in the following more illustrative image, as shown in Figure 13.

We can start to see that most points in the plane are in the domain of attraction, except for the important point $(\pi, 0)$. As alluded to before, this is an unstable equilibrium point of the system, and therefore will not converge to the origin. Because this is a point and therefore has measure zero, as we continue to perform this integration the set will become more dense around this point, but no flows will intersect this specific point, as seen in Figure 14. In an attempt to due the geometry of the system justice, in Figure 15 we have this final plot showing the solutions in the true phase space, $\mathbb{S} \times \mathbb{R}$.

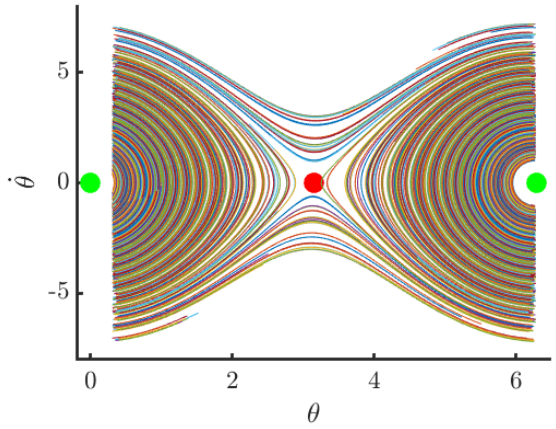

Figure 13: Ω_1 under modified geometry.

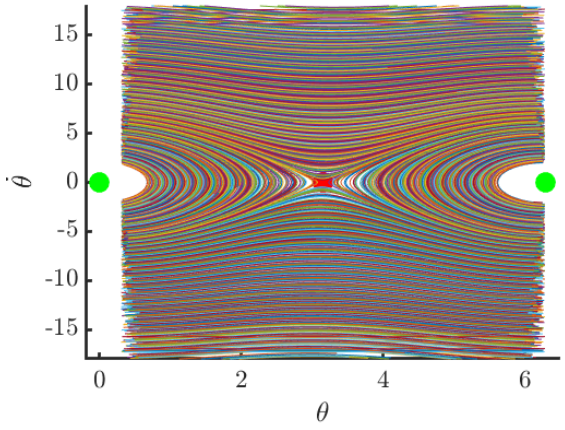

Figure 14: Ω_2

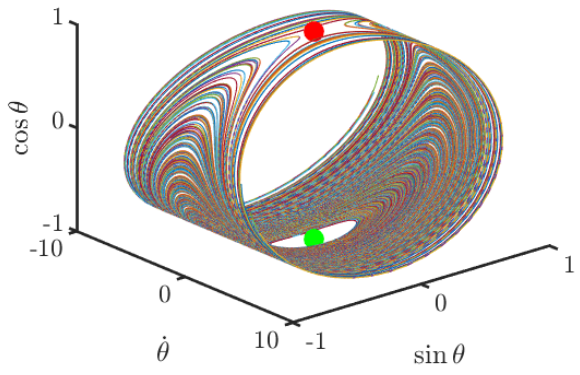

Figure 15: Ω_1 under the correct geometry.

9 Underactuated Periodic Orbits

For the final piece of this project, periodic orbit generation for the triple pendulum is investigated. In order to sneak some controls into this project, and to combat the nonconservative damping, the system is such that the first link of the triple pendulum is actuated. The initial condition

$$x_0 = \begin{bmatrix} \frac{\pi}{4} & \frac{\pi}{4} & 0 & 0 & 0 & 0 \end{bmatrix}$$

is chosen arbitrarily, and an optimization problem is run in order to find the control input required to generate a periodic orbit, as given by

$$\begin{aligned} \min_{u\in\mathcal{B},\ T\in\mathbb{R}_{>0}} \quad & \|u\|_2 \\ \text{s.t.} \quad & \dot{x} = f(x) + g(x)u \\ & \varphi_{t+T}(x_0) = \varphi_t(x_0) \end{aligned} \tag{2}$$

where $\mathcal{B}$ is the set of 10^{th} order Bézier polynomials. The optimization problem in 2 converged in 43 iterations after 40.8 seconds and terminated with a feasibility of 7.039e-11. In order to investigate the stability of the orbit, the method of Poincaré sections is used, with a Poincarè section given by

$$\Sigma = \{x \in \mathbb{R}^{2n} : (x_0 - x)^\top f(x_0) = 0\}.$$

The above form was constructed numerically, and set as an ODE event function to stop integration upon satisfaction. Because a hyperplane was used instead of a more intelligently designed hypersurface, the system intersected the plane with the valid velocity condition twice per period, so extra care was taken to ensure that the condition only stopped integration when desired.

Perturbing the system and constructing a linearization of the Poincarè return map results in a range of eigenvalues above and below 1. The validity of the linearization method is verified by noting that none of the eigenvalues are exactly 1. The absolute value of the largest eigenvalue of the discretized Poincarè section is 1.023, meaning nothing can be concluded about the stability of the system. It was clear to see through simulation though that the system was unstable. In fact, even without perturbations the optimized orbit was found to diverge, as seen here.

What is perhaps more interesting, is that by leaving the system to evolve further, the forced triple pendulum converges to a period-2 orbit. The stability of this new orbit is then investigated using the same method of Poincarè sections, and similar to before, a range of eigenvalues above and below 1 are found, with the maximum eigenvalue being given by

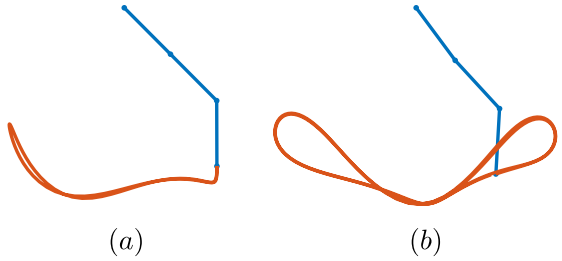

Figure 16: Physical evolution of the system with path shown in orange. (a) depicts the nominal periodic orbit that was optimized for and (b) depicts the orbit that the system converged to after 200 seconds.

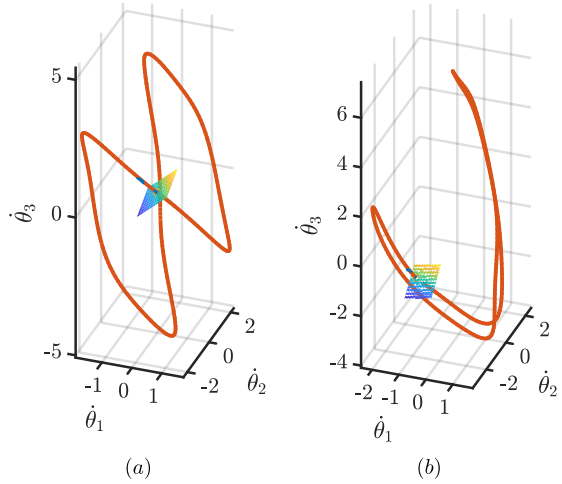

Figure 17: Evolution of the system in velocity space. (a) depicts the nominal periodic orbit that was optimized for and (b) depicts the orbit that the system converged to after 200 seconds.

4.76. Although again nothing can be definitively concluded, using similar logic as before could lead us to (erroneously) believe that this orbit is highly unstable. However, the only thing we can conclude with the linearized Poincarè section is that the system is not exponentially stable. If we again leave the system to run, we notice that the trajectory eventually converges back to the desired orbit. This would naturally lead to the conjecture that the new orbit is asymptotically stable, but we unfortunately do not posses the numerical tools to prove such a statement. The evolution of the system as a physical system and in velocity space can be seen in Figures 16 and 17, respectively. One explanation for the stability of the new orbit comes from looking at the energy of the system over time, as seen in Figure 18, where the system naturally flows to a minimal energy state of period-2 nature.

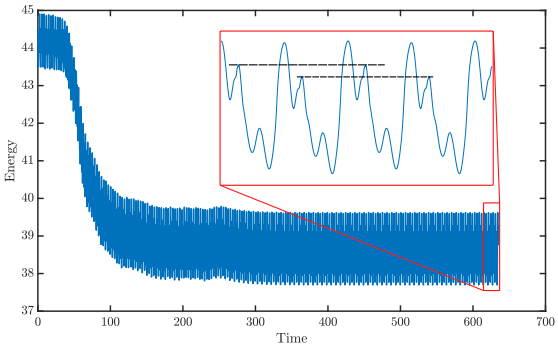

Figure 18: Flow of system to minimal energy state of period-2 nature.

This phenomena raises a number of questions, each of which would be interesting to investigate further. First, why does the system "prefer" the orbit that it converged to? Is the energy a complete explanation, and is the fact that the stable orbit has greater symmetry a coincidence? Next, how can we exploit the stability property of the second orbit into our original trajectory generation program? Finally, how can we incorporate feedback to render our original optimized orbit attractive?

As a further research goal, I would like to more rigorously investigate switching between periodic orbits. A preliminary theory for this exists in dynamics literature, namely in the field of homo/heteroclinic connections between periodic orbits, but I have not seen this properly formulated in the control theory literature. What we have just created, in fact, is controller which creates a homoclinic connection between two orbits, as depicted in Figure 19. A potential research question could go as follows: Can we create a switching controller with stability guarantees to create homo/heteroclinic connections between periodic orbits? Essentially, how can we predict and control the behaviour we have just discovered?

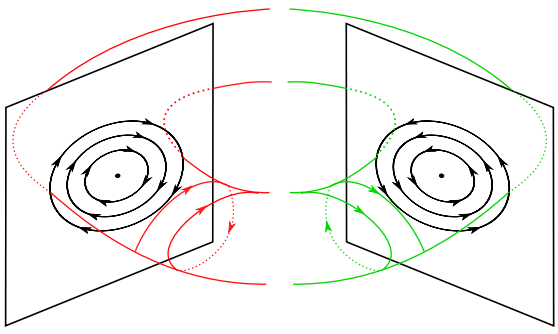

Figure 19: Heteroclinic connection between two periodic orbits.

10 Appendix: Derivation of EoM

Let s_i be the spatial reference frame of the i^{th} body, with s_0 representing the global origin (located at the center of the fixed base) by convention. Additionally, let m_i, b_i, and l_i represent the mass, damping, and length of the i^th link, respectively. If $\mathbf{r}_{i,j} \in \mathbb{R}^n$ represents the location of the j^{th} body in the i^{th} reference frame, we have

$$\mathbf{r}_{i-1,i} = \begin{bmatrix} l_i \sin\theta_i & l_i \cos\theta_i \end{bmatrix}$$

and

$$\mathbf{r}_{0,i} = \sum_{j=1}^{i} \mathbf{r}_{j-1,j}.$$

With $\mathbf{v}_i \in \mathbb{R}^2$ representing the velocity of the i^{th} body in the global frame, we can calculate

$$\begin{aligned} \langle \mathbf{v}_i, \mathbf{v}_i \rangle &= \mathbf{r}_{0,i} \cdot \mathbf{r}_{0,i} \\ &= \left(\sum_{j=1}^{i} \mathbf{r}_{j-1,j} \right) \cdot \left(\sum_{j=1}^{i} \mathbf{r}_{j-1,j} \right) \\ &= \sum_{j=1}^{i} \sum_{k=1}^{i} l_j l_k \dot{\theta}_j \dot{\theta}_k \cos(\theta_j - \theta_k). \end{aligned}$$

With this we can construct the kinetic energy of the system, T, as

$$T = \frac{1}{2} \sum_{i=1}^{n} m_i \langle \mathbf{v}_i, \mathbf{v}_i \rangle.$$

We can also describe the vertical height of the i_{th} link is the world frame as

$$\begin{aligned} h_i &= \langle \mathbf{r}_{0,i}, \hat{\mathbf{j}} \rangle \\ &= \sum_{j=1}^{i} \langle \mathbf{r}_{j-1,j}, \hat{\mathbf{j}} \rangle \\ &= \sum_{j=1}^{i} l_j \cos\theta_j \end{aligned}$$

leading to the potential energy of the system, V, as

$$V = g \sum_{i=1}^{n} m_i h_i.$$

Our Lagrangian, of course, is simply $L = T - V$. We can now use the Lagrange-d'Alembert principle to get the equations of motion as

$$\frac{d}{dt} \left(\frac{\partial L}{\partial \dot{\theta}_i} \right) - \frac{\partial L}{\partial \theta_i} = b \dot{\theta}_i$$

$$\begin{aligned} l_i^2 \ddot{\theta}_i \sum_{j=1}^{n} m_j + l_i \sum_{j=1}^{n} \sum_{k=\max\{i,j\}}^{n} l_j m_k (\ddot{\theta}_j \cos(\theta_i - \theta_j) - \dot{\theta}_j (\dot{\theta}_i - \dot{\theta}_j) \sin(\theta_i - \theta_j))(1 - \delta_{ij}) \\ - g m_i \sum_{j=1}^{i} l_j \sin\theta_i + l_i \dot{\theta}_i \sum_{j=1}^{n} \sum_{k=\max\{i,j\}}^{n} l_j \dot{\theta}_j m_k \sin(\theta_j - \theta_i)(1 - \delta_{ij}) = b \dot{\theta}_i \end{aligned}$$